Tectonophysics 733 (2018) 171–181

Contents lists available at ScienceDirect

Tectonophysics

journal homepage: www.elsevier.com/locate/tecto

Review Article

Geotribology - Friction, wear, and lubrication of faults

Yuval Boneh[a,b,*], Ze'ev Reches[c]

[a] Washington University in St. Louis, Earth and Planetary Sciences, Saint Louis, MO 63130, USA
[b] Brown University, Department of Geological Sciences, Providence, RI 02912, USA
[c] Oklahoma University, School of Geology and Geophysics, Norman, OK 73190, USA

ARTICLE INFO

Keywords:
Geotribology
Fault gouge
Friction
Wear
Lubrication

ABSTRACT

We introduce here the concept of Geotribology as an approach to study friction, wear, and lubrication of geological systems. Methods of geotribology are applied here to characterize the friction and wear associated with slip along experimental faults composed of brittle rocks. The wear in these faults is dominated by brittle fracturing, plucking, scratching and fragmentation at asperities of all scales, including 'effective asperities' that develop and evolve during the slip. We derived a theoretical model for the rate of wear based on the observation that the dynamic strength of brittle materials is proportional to the product of load stress and loading period. In a slipping fault, the loading period of an asperity is inversely proportional to the slip velocity, and our derivations indicate that the wear-rate is proportional to the ratio of [shear-stress/slip-velocity]. By incorporating the rock hardness data into the model, we demonstrate that a single, universal function fits wear data of hundreds of experiments with granitic, carbonate and sandstone faults. In the next step, we demonstrate that the dynamic frictional strength of experimental faults is well explained in terms of the tribological parameter PV factor (= normal-stress · slip-velocity). This factor successfully delineates weakening and strengthening regimes of carbonate and granitic faults. Finally, our analysis revealed a puzzling observation that wear-rate and frictional strength have strikingly different dependencies on the loading conditions of normal-stress and slip-velocity; we discuss sources for this difference. We found that utilization of tribological tools in fault slip analyses leads to effective and insightful results.

1. Introduction: tribology and geotribology

Tribology was established as a discipline by Jost (1976) report, and later Bowden and Tabor (1973) stated: "The study of friction demands an interdisciplinary approach because friction is the result of a number of interacting processes. Although friction is simple to measure, it is complicated to explain. … as a result of increased interest in friction, lubrication, and wear, a new word has been coined to describe the field: tribology. This word derived from the Greek tribos, which means 'rubbing.' Tribology is defined as 'the science and technology of interactive surfaces in relative motion and of the practices relating thereto'." The integrated effects of friction, wear, and lubrication at the interface have a strong impact on the functionality of machinery with major economic consequences. Thus, most tribological studies were conducted within the fields of mechanical engineering and material sciences with thousands of publications in the 15 (!) journals devoted to tribology and wear. However, slipping bodies are not restricted to machinery, and tribological concepts were adopted outside pure technology, as noted by Kato (2014) that "…. the expressions of 'Space & aero-, Vehicle-, Process-, Information-, Storage-, Maintenance-, Bio-, Nano-, Eco-, and Geo-tribology' have been introduced …".

The term 'geotribology' was first mentioned by Blok (1963) with no discussion. Enomoto (2005) noted the lack of mutual research between seismology and tribology despite their apparent similarities, and Dove and Jarrett (2002) used a geotribology framework to analyze the flow mechanics of granular sand. However, even though tribological concepts can be applied to many geosciences phenomena, the two research communities are separated. For example, out of about 26,000 publications in the tribology/wear journals, only 15 mentioned earthquakes, and out of almost 100,000 publications in leading geology/geophysics journals, only two (!) refer to tribology, whereas about 1000 publications analyzed friction and wear.

We follow previous studies (Dove and Jarrett, 2002; Enomoto, 2005; Kaneko, 2000), and propose here to utilize 'geotribology' as an interactive framework for the analysis of geologic processes of bodies at relative motion involving friction, wear, and lubrication. Faulting and earthquake processes are clear geotribological phenomena, but the tribological approach is also relevant to glacier flow (Beeman et al.,

* Corresponding author at: Brown University, Department of Geological Sciences, 324 Brook St, Providence, RI 02912, USA.
E-mail address: yuval_boneh@brown.edu (Y. Boneh).

https://doi.org/10.1016/j.tecto.2017.11.022
Received 31 July 2017; Received in revised form 30 October 2017; Accepted 18 November 2017
Available online 12 December 2017
0040-1951/

1988; Lee and Rutter, 2004), landslide creep (Brodsky et al., 2003; Goren and Aharonov, 2007), debris flow (Iverson, 1997), stream-bed erosion (Karimi and Schmid, 1992), volcanic eruption and lava flow (Ferlito and Siewert, 2006). Indeed, many components of tribology were used in earth sciences, particularly in rock friction analyses. For example, Dieterich (1979) and Dieterich and Kilgore (1994) applied the asperity-asperity contact mechanism of Bowden and Tabor (1964) to rock friction experiments that led to the rate- state- friction law which prevails in earthquake analyses (Marone, 1998). Reches and Lockner (2010) applied the powder lubrication analysis of Heshmat (1991) to explain fault weakening at high slip-velocities and Boneh et al. (2013) used the three-body concept of Godet (1984) for the interpretation of fault wear processes. The concept of flash heating that was developed by Blok (1940, 1963) was adopted to fault dynamic weakening by Rice (2006).

To demonstrate the geotribological approach, we present here a critical review of wear and friction along brittle faults. In the first part, we examine the wear model of Archard (1953), which is based on failure at contacting asperities, and review wear mechanisms observations. Then, following Godet (1984) concept of shear along a 'three body' system, we consider the effective asperity model. The present compilation of wear-rates along experimental rock faults indicates a strong dependency on slip-velocity that was not considered in Archard model. To incorporate slip-velocity, we derive a wear model that integrates loading conditions, mechanical properties, and contact conditions. In the second part, we compiled the dynamic frictional strength in rock shear experiments, and find that it depends simultaneously on multiple properties of the tribological system. Based on these reviews, we discuss the relations between fault wear and fault friction.

2. Wear of brittle faults

2.1. Wear mechanisms

In general, a tribological system is defined by its blocks properties (e.g., cohesion, composition, and interface geometry), loading conditions, environmental conditions, and the characteristics of the layer separating the surfaces (e.g., lubricating agent) (Fig. 1). A fault is a distinct example of a geotribological system where slip is always associated with frictional resistance and wear. Friction and wear are intrinsically linked to each other and both have complex dependence on the properties of the fault system (Rabinowicz, 1965). The complexity of the wear can be demonstrated by the multiple wear mechanisms of the interacting blocks: (1) Adhesive wear at asperity-to-asperity contacts controlled by the plastic strength at the asperities scale (Archard, 1953); (2) Abrasive wear in which a harder material (or particle) penetrates and ploughs the facing surface (Moore and King, 1980; Rabinowicz et al., 1961); (3) Delamination wear in which the load at asperities contact damages the interior of the sliding blocks (Fleming and Suh, 1977; Suh, 1973); (4) Fatigue and fretting wear in which repeated sliding with subsurface fracturing causes sever wear (Kato, 2002; Rozeanu, 1963); and (5) Corrosive wear due to chemical reactions that weaken the blocks strength around the slip surface (Watson et al., 1995). These wear mechanisms can act simultaneously, and the active mechanisms can be identified by microscopic and ultramicroscopic analyses (e.g., Hsu and Shen, 2004). The global wear, which is the sum of all mechanisms in the specific tribological system, is often measured macroscopically by continuous monitoring the experimental parameters or by sporadic measurements (Boneh et al., 2013).

The basic model for the global wear, which was proposed by Archard (1953), states that the wear amount during slip, W, is related to the material properties, normal stress, and displacement through the Archard equation:

$$W = K(\sigma/H)d \quad (1)$$

where K is a constant, σ is the normal stress, d is the displacement, and H is the material hardness. Later, Queener et al. (1965) demonstrated that Archard model fits the steady-state conditions, but during the early stage of slip, referred to as 'running-in', the wear-rate is significantly higher. Archard's model ignores the effect of slip velocity, and it was recently demonstrated that this effect is particularly strong for rock faults (Boneh et al., 2013; Hirose et al., 2012). This shortcoming of the Archard's model is eliminated in the analysis below.

2.2. Asperities and effective-asperities

In general, wear occurs by failure at contacting asperities which are sites of high, local stresses (Archard, 1953) as the real contact area is a small fraction of the nominal blocks area (Bowden and Tabor, 1939). In manufactured metallic elements, the asperities are micron-scale features defined by the surface roughness, and they are likely to fail by plastic deformation (Archard and Hirst, 1956). Rocks, however, are more brittle than metals (about an order of magnitude lower fracture toughness for rocks) and their asperities are more likely to fail by fracturing and fragmentation (Byerlee, 1967). Our analysis is devoted to wear by brittle fracturing of asperities.

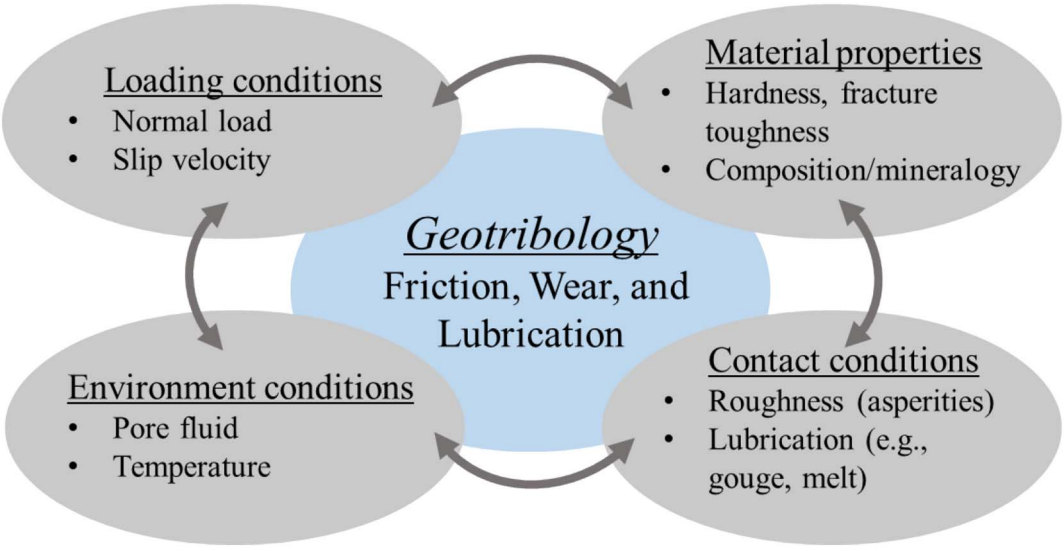

Fig. 1. Conceptual interaction between mechanical processes and loading conditions that control wear, friction, and lubrication in a geotribological system.

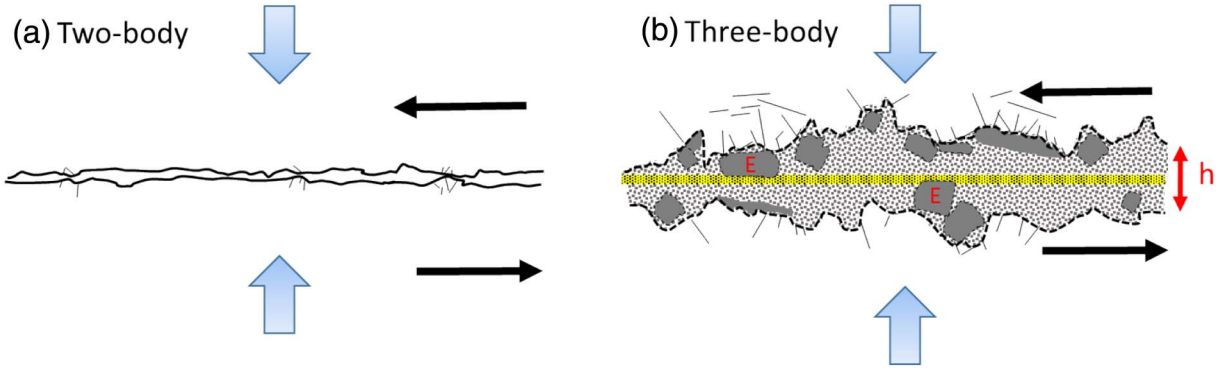

Fig. 2. Simplified view of the contact between two loaded fault blocks. (a) Two-body fault with two bare blocks in direct contact only at touching isolated asperities. (b) Three-body fault-zone in which the two are separated by a gouge layer composed of fine grains at the nanometer to micron scale (dotted yellow), as well as large particles (dark grey). The large particles control the effective asperities (E') that generate local stress and wear, whereas the flow of the fine grains control the friction (Reches and Lockner, 2010).

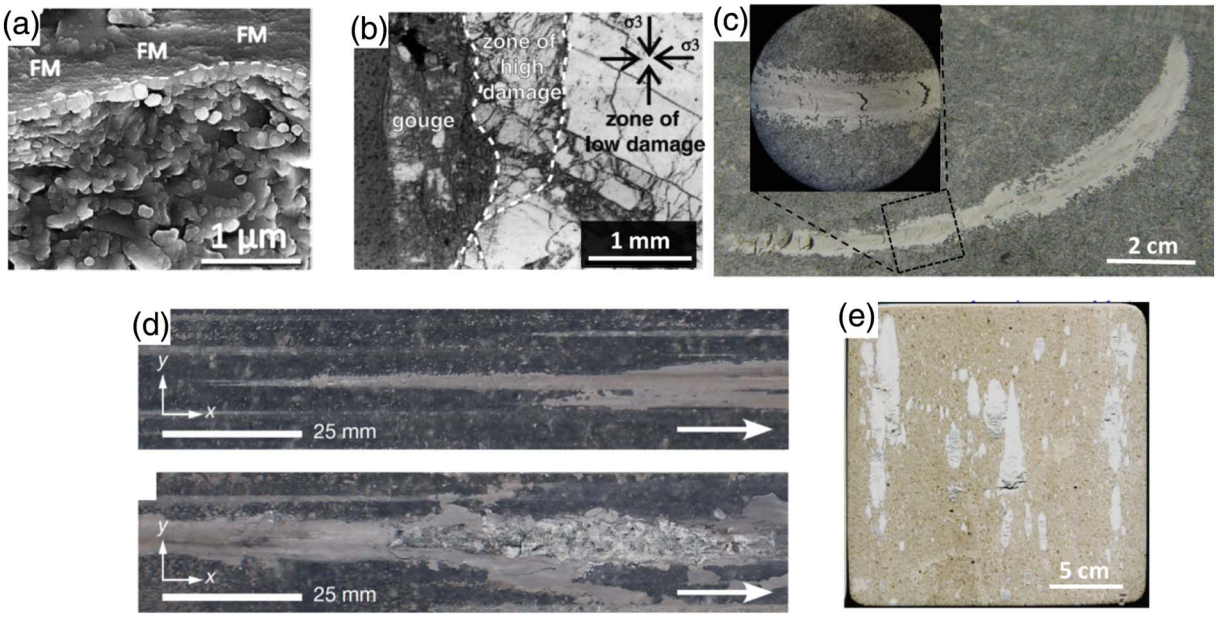

Fig. 3. Close-up of experimental faults slip surfaces displaying damage by asperities at various scales (see text). (a) Nanoscale in limestone (Siman-Tov et al., 2015). (b) Sub-mm scale in granite (Amitrano and Schmittbuhl, 2002). (c), (d) and (e) cm-scale in quartzite (Boneh, 2012), metagabbro (Yamashita et al., 2015), and limestone (Tesei et al., 2017) respectively.

Examination of experimental rock faults reveals two general styles of wear features. In the first wear style, two-body mode (Fig. 2a), the wear is localized at isolated asperities that induce small scale failure by fracturing, plucking, abrasion, and smearing (Boneh et al., 2014; Engelder, 1974; Hundley-Goff and Moody, 1980; Power et al., 1988; Yamashita et al., 2014). This localized wear is associated with striations of finite length that is approximately equal to the slip-distance (Boneh et al., 2014), as well as by isolated, lensoidal zones of smeared powder (Fig. 3d) (Engelder, 1974; Yamashita et al., 2015). The two-body mode wear is therefore characterized mostly by interactions at isolated asperities (Fig. 2a) (Godet, 1984).

The second wear style, three-body mode, occurs while the fault is covered by a continuous gouge layer of finite thickness (Boneh et al., 2013; Reches and Lockner, 2010). The gouge layer separates the two fault locks, and prevents direct contact between the isolated asperities of the fault blocks (Fig. 2b). This configuration transfers the system from two-body mode to three-body mode (Boneh et al., 2014; Godet, 1984). Under this mode, the wear occurs at the contacts between the gouge and the host blocks (Lyakhovsky et al., 2014), and the gouge thickens by fracturing and plucking the host block. The plucked particles integrate into the gouge, and can be much larger than the initial surface roughness (Boneh et al., 2014; Brown and Fialko, 2012; Renard et al., 2012; Yamashita et al., 2015). This process modifies the nature of contact between the gouge layer and the host rock with multi-scale roughness (Sagy et al., 2017); we refer here to the asperities at the gouge-rock interface as 'effective asperities'.

The effective asperities differ from the initial asperities at rock-rock contact by size. The asperities of a polished rock surface, which is the initial stage in most experimental analyses, are on the order of 1–10 μm, while plucked material and associated pits of the sub-slip surface fracturing generate asperities on the order of mm to cm in size (e.g., slip features in Fig. 3). Further, field analyses revealed effective asperities with large amplitude and wavelengths of tens of meters (Sagy and Brodsky, 2009; Sagy et al., 2007). Naturally, the effective asperities along the fault zone are sites of stress concentration (Candela et al., 2011; Chester et al., 1993) and thus, act as the sites of intense local fracturing and wear. The wear mechanism associated with effective asperity at gouge-rock contact is the sub-surface fracturing of the rock block (Fig. 3d; Boneh, 2012; Jackson and Dunn, 1974; LaFountain et al., 1975; Suh, 1973). The fracturing facilitates the removal of rock fragments from the fault blocks, and modification of the effective roughness with slip (Shervais and Kirkpatrick, 2016; Tesei et al., 2017). The effective roughness is therefore fundamentally different from the original surface roughness by its failure mechanism and scale. Based on

Table 1
List of studies and their range of mechanical conditions used to construct the wear data for Figs. 4 and 5.

	Apparatus	Lithology	Normal stress [Mpa]	Velocity [mm/s]	Displacement	Wear measurements	Notes
Boneh et al. (2013); Boneh and Reches (2016)	Rotray shear	Sierra White granite; Kasota Dolomite	0.5–7	1–1000	1–10 m	Axial shortening during slip	
Hirose et al. (2012)	Rotary shear	Inada granite; Calcareous sandstone	0.2–6.3	4–270	6–220 m	Axial shortening during slip	
Wang and Scholz (1994)	Rotary shear	Westerly granite	1–10	0.15	1.5–2.0 m	Gouge collected and weighted.	WR was calculated using granite density of 2.7 g/cm^3 and friction coefficient of 0.7.
Yoshioka (1986)	Biaxial	Makaba granite; Choshi sandstone	4–110	0.2–1	5–15 mm	Gouge collected and weighted.	Velocity is averaged. WR was calculated using densities of 2.7 and 2.5 g/cm^3 for granite and sandstone, respectively.
Badt et al. (2016)	Biaxial	Hebron limestone	5–15	0.05	1 cm	Wear volume was estimated by the change of roughness due to slip.	Volume wear was converted to units of wear-rate with slip area and slip distnace.
Teufel (1981)	Triaxial	Coconino sandatone	~200	0.019	up to 8 mm	Gouge thickness was observed in slip surface thin sections.	

these observations, we envision that the effective roughness is a dynamic, time-dependent feature of a fault that controls the wear and damage of the fault blocks.

2.3. Experimental wear-rates

Continuous quantification of the wear-rate during fault sliding can be accomplished by monitoring the fault-normal displacement with correction of thermal effects (Boneh et al., 2013). The wear-rate data is presented by fault-normal shortening due to wear relatively to slip-distance with units of μm/m. The wear-rate data was compiled from 142 experiments with faults composed of granites, carbonates and sandstones. Shear conditions ranged widely: normal stress of 0.25–203 MPa and slip-velocity of 10^{-5}–1 m/s (Table 1). The experiments were performed in three setups: (1) Rotary shear apparatus that allows for unlimited slip distance, high velocities (up to 1 m/s), and low to moderate normal stresses (0.25–7 MPa). Wear was measured as fault-normal shortening that indicates the volume of ejected gouge (Boneh et al., 2013; Hirose et al., 2012), or by weighing the produced gouge (Wang and Scholz, 1994). The main shortcoming of this setup is that the worn material, unlike gouge in faults, can be ejected from the slip surface; (2) Direct shear apparatus with limited capability for slip distance, and high normal stress (tens to hundreds MPa). Wear-rate is measured by removing the gouge from the fault zone and weighting it (Yoshioka, 1986), or by comparing the fault surface geometry before and after the experiment (Badt et al., 2016); (3) Triaxial apparatus which allows high normal loads and confining pressure while limited slip distance (up to cm) and velocity (10^{-5} m/s). Wear was estimated using thin sections of the fault zone (Teufel, 1981).

We examined the relations between the recorded steady-state wear-rates and the experimental conditions of slip slowness (= 1/slip-velocity) (Fig. 4, left), applied normal stress (Fig. 4, center), and the ratio shear-stress/slip-velocity (Fig. 4, right). The figure indicates power relations between the measured wear-rates and the applied experimental conditions for a few orders of magnitude. The better fit (R^2 = 0.86–0.93) is for wear-rate, WR, as function of the ratio [shear-stress/slip-velocity] (Fig. 4, right),

$$WR = a\cdot(\tau/V)^b \quad (2)$$

where τ is the shear stress, V is slip velocity, and a and b are material constants. We note here that the power b is about 1 for all rock types. This relation between wear-rate and [stress/velocity] is well explained by the wear model derived below.

3. A model of wear mechanics of brittle faults

Recent analyses of wear along experimental faults provided systematic relations between the measured wear-rates, the applied load, and the slip-velocity for faults made of granites, carbonates, and sandstones (Fig. 4) (Boneh and Reches, 2016). Here, we use these relations to derive a general model of the wear-rate of brittle faults. It is demonstrated that the wear-rate is controlled by the mechanical impulse of the fault system; mechanical impulse is the product of the loading-force and the loading-time, as detailed below. In this section, the model is developed in three steps: (1) outline of the central mechanical concepts of the model; (2) model derivation; and (3) application to the experimental data.

3.1. Mechanical impulse: the controlling parameter of fault wear

Many studies revealed that brittle wear is facilitated by fracturing at contacting asperities in two-body mode (Fig. 2a) and at effective asperities under the three-body mode (Fig. 2b) (Dunn et al., 1973; Hutchings, 1992; Jackson and Dunn, 1974; Moore and King, 1980; Yamamoto et al., 1994). The localization of wear at asperities of multiple scales is expected due to intense stress amplification at asperities

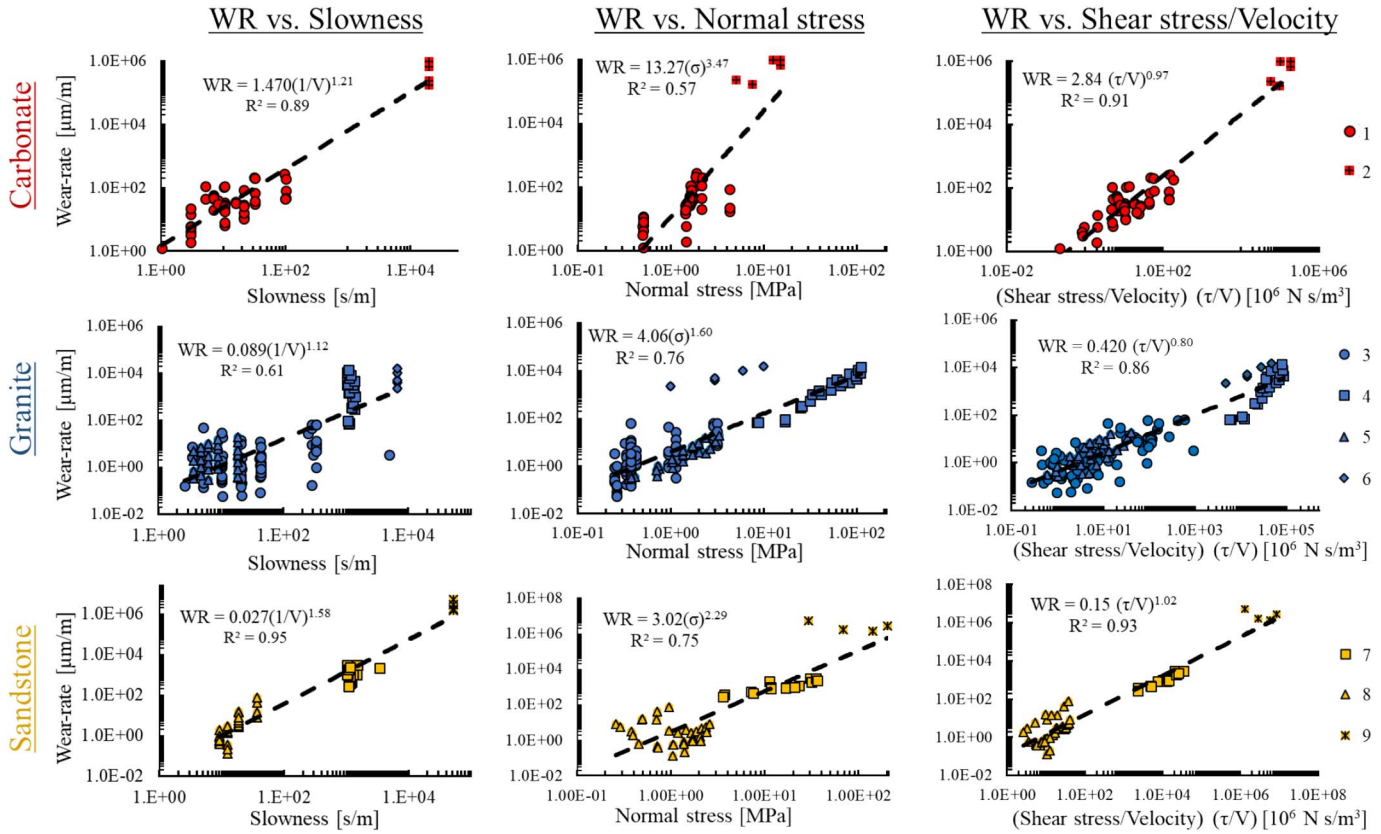

Fig. 4. Experimental wear-rates of carbonates (upper row, red), granites (center row, blue), and sandstones (lower row, yellow) as a function of slip-slowness (left column), normal stress (center column), and the ratio (shear stress/slip velocity) (right column). Data sources (Table 1): 1 – Boneh et al., 2013; Kasota dolomite; 2 – Badt et al., 2016; Hebron marble; 3 – Boneh and Reches, 2016; Seirra White granite; 4 – Yoshioka, 1986; Makaba granite; 5 – Hirose et al., 2012; Inada granite; 6 – Wang and Scholz, 1994; Westerly granite; 7 – Yoshioka, 1986; Choshi sandstone; 8 – Hirose et al., 2012; Calcareous sandstone; 9 – Teufel, 1981; Coconino sandstone.

(Chester et al., 1993; Lawn, 1975; Scholz, 1987). The experimental data presented in Fig. 4 showed that the wear-rate of carbonates, granites, and sandstones faults have systematic, power relations to the loading conditions (Eq. (2)). The observations of wear at asperities and the power relations serve as the basis for the present model.

We postulate that wear-rate variation reflects the strong dependence of dynamic brittle fracturing on loading rate. Examples of the strength dependence of brittle materials on the applied strain-rates are the increase of strain-rate that leads to strength increase (Goldsmith et al., 1976; Lindholm et al., 1974), and the increase of loading-rates that leads to the increase of material toughness (Zhang and Zhao, 2013, 2014; Zhang et al., 1999). Related observations had been recognized as part of the tribological properties of ceramics: Up to a critical velocity (on the order of $V > 1$ m/s) increase of slip-rate is, counterintuitively, associated with a decrease of wear-rates (Al-Qutub et al., 2008; Bai et al., 1996; Conway et al., 1988; Hsu and Shen, 1996; Subramanian, 1991; Zhang and Alpas, 1997).

In line of these observations, it was found that brittle strength is proportional to both load magnitude and load duration (Bouzid et al., 2001; Qian et al., 2009; Shockey et al., 1986; Tuler and Butcher, 1968). Tuler and Butcher (1968) and Barker et al. (1964) found that the tensile strength of aluminium samples dropped with increasing loading duration. They attributed the strength drop to damage accumulated during the loading period. They proposed that under constant stress, the tensile strength, G, is related to the loading-time as:

$$G = \Delta t \cdot \sigma^{\lambda} \quad (3)$$

where Δt is the loading period, σ is the applied stress, and λ is a material constant. This relation suggests that the strength is related to mechanical impulse, J, which is the product of force, F, and loading period Δt,

$$J = \Delta t \cdot F \quad (4)$$

for a constant force loading. The impulse J is used, for example, in the analyses of body impact and momentum conservation. For the present analysis, we use the impulse density, $\hat{J}$, which is the mechanical impulse per unit area,

$$\hat{J} = J/A = \Delta t \cdot \sigma \quad (5)$$

Eqs. (3) and (5) suggest that the dynamic tensile strength, G, of fault blocks is proportional to the impulse density, $\hat{J}$,

$$G \propto \hat{J} \quad (6)$$

Following the above observations that rock wear is governed by fracturing and fragmentation at asperities, we now postulate that the rate of wear is controlled by the rate of dynamic fracturing and the time-dependent rock strength (G). Since G is proportional to the impulse density, $\hat{J}$, the fracturing at the asperities would be proportional to the density of the mechanical impulse. This relation between the impulse-density and asperities strength is now used for the derivation of a velocity dependent wear model describing wear through the integrated force over time (i.e., impulse) acting on an asperity.

Consider two fault blocks of nominal area A that contain n asperities of mean dimension L and area L^2. When the blocks slip with respect to each other, the contact period, Δt, at an asperity is inversely proportional to the slip velocity, and at any given point on the fault, the period is the slip-slowness (1/V) times the asperity length, L,

$$\Delta t = L/V \quad (7)$$

The shear force on the average asperity is

$$F_a = \tau \cdot A/n, \quad (8)$$

where τ is the shear stress. The mechanical impulse on the average

asperity is

$$J = F_a \cdot \Delta t = \tau \cdot A \cdot L/V \cdot n. \quad (9)$$

The impulse density on the entire fault

$$\hat{J} = J \cdot n/A = L \cdot (\tau/V) \quad (10)$$

Based on the time-dependence of brittle strength (Eq. (3)), the fracturing would be proportional to the mechanical impulse on asperities (Eq. (6)). As the wear-rate is proportional to the fracturing-rate, we deduce that the fault wear-rate will be proportional to the impulse density on the fault. Therefore,

$$WR \propto \hat{J} = C\,(\tau/V) \quad (11)$$

where C is a constant that incorporates the rock strength and the asperities dimensions. Below we apply this model to the experimental data.

3.2. Model investigation

The above model is based on one, observation-based assumption: the wear of brittle faults is controlled by dynamic fracturing and fragmentation at fault asperities. Using the time-dependence of dynamic fracturing, we derived the dependence of the wear-rate on the ratio [shear-stress/slip-velocity]. The model prediction (Eq. (11)), that was derived independently from the experimental observations (Fig. 4), is now compared to the experimental relations.

The wear model is based on fracturing failure at asperities, and thus, the K parameter in Eq. (1) is envisioned as a measure of the failure tendency of the fault blocks. Following Archard (1953), we select C to be the inverse of rock hardness, namely,

$$C = K/H \quad (12)$$

where H is hardness and K is constant from Archard equation (Eq. (1)), which functions as a unit scaling parameter. Hardness, with units of GPa, is measured in indentation tests in which the extent of permanent deformation is related to the applied local compressive loading (Bishop et al., 1945). Hardness indicates the material competence by integrating multiple mechanical properties including strength, elasticity, plasticity, brittleness, and viscoelasticity. It was also found that wear is inversely related to hardness, particularly in brittle materials that undergo abrasive wear (Adachi and Hutchings, 2005; Archard, 1953; Engelder and Scholz, 1976; Rabinowicz et al., 1961; Srinivasan and Scattergood, 1988; Zum Gahr, 1988). Combining Eqs. (11) and (12) yields the model wear-rate formula.

$$WR_H = WR \cdot H = K \cdot (\tau/V) \quad (13)$$

in which WR_H is regarded as the normalized wear-rate.

In this analysis, we used microindentation hardness for quartz (14.5 GPa), orthoclase (9.1 GPa) and calcite (2.2 GPa) (Broz et al., 2006). For the carbonates and sandstones data, we used the hardness of calcite and quartz, respectively, and for the granite data we used the average hardness of quartz and orthoclase (11.8 GPa). The wear-rate data of the three analyzed lithologies (Fig. 2) collapse to single power curve (Fig. 5a) of the form

$$WR_H = (5.03 \pm 0.6) \cdot (\tau/V)^{0.88 \pm 0.02};\ r^2 = 0.878. \quad (14)$$

This result leads to two deductions. First, the power of b = 0.88 is close to unity, and thus it is in general agreement with the linear relation predicted by the theoretical model (Eq. (13)). Second, the hardness of the fault blocks appears as the dominant, universal factor in controlling the wear-rate of brittle faults (Fig. 5a), whereas, other fault properties, e.g., roughness spectrum and amplitude, that are not included in the normalization appear to have only secondary effect.

Once this relation (Eq. (14)) is established, we use the normalized wear-rate data to plot the wear-rate values in space of slip-velocity and normal stress (Fig. 5b). This plot is a wear-map that is used in tribology to bound the intensities of wear and friction as function of the relevant loading conditions (Adachi et al., 1997; Ashby and Lim, 1990; Hsu and Shen, 1996; Lim and Ashby, 1987). We adopted this mapping method in the analysis of carbonate faults (Boneh et al., 2013) and the friction of talc gouge (Chen et al., 2017a). The wear-map in Fig. 5b indicates three wear regimes: gentle wear-rates (blue symbols) under high slip-velocity ($V > 0.001$ m/s) and low normal stress ($\sigma_n < 4$ MPa), moderate to severe wear-rates (green – yellow symbols) under $0.0001\ \text{m/s} < V < 0.001$ m/s and $3\ \text{MPa} < \sigma_n < 100$ MPa, and severe wear-rates (red symbols) at $V < 0.0001$ m/s and $\sigma_n > 150$ MPa. The three wear regimes are separated by lines of constant ratio of σ_n/V (grey dashed lines).

The model derived above (Eq. (14), Fig. 5a) incorporates the effects of fault strength (via hardness), and loading conditions (normal and shear stresses, and slip-velocity) for three different lithologies and over six orders of magnitude. Therefore, we regard it as a universal, geotribological model of fault wear. Considering the wide range of the loading conditions of the experimental data that fit the model, we envision that the model predictions can be used to evaluate the wear-rates of experimental and field faults.

4. Dynamic frictional strength of faults

The dynamic weakening of faults during seismic slip motivated many analyses of shear along experimental faults at high velocity (e.g., Di Toro et al., 2004; Tsutsumi and Shimamoto, 1997). Typically, this weakening was presented in diagrams of friction coefficient, μ, as function of the steady-state slip-velocity, V (Reches and Lockner, 2010). It was later proposed that μ can be analyzed in relationship with the power-density, PD, (Boneh et al., 2013; Di Toro et al., 2011; Liao et al., 2014).

$$PD = \tau \cdot V \quad (15)$$

Power-density, with units of MW/m^2, is a measure of the rate of energy dissipation during shear, and thus, is viewed as a good indicator of frictional strength. However, as the frictional strength, τ, evolves during fault slip, the power-density also evolves during slip, and thus, PD is not a constant loading parameter even during a constant velocity experiments. Following tribology practices, we utilize here the PV-factor, which is the product of pressure, P, and slip-velocity, V (Enomoto et al., 1993; Williams, 2005). The PV-factor is typically used to quantify the quality of a frictional system, and the critical PV is the maximum loading condition that the system can support without severe damage (Ramalho and Miranda, 2006). In the present analysis of fault friction, we apply the PV-factor as.

$$PV = \sigma_n \cdot V \quad (16)$$

with similar units to the PD, MW/m^2. As σ_n does not change significantly during fault shear, the PV-factor is likely to directly represent the effect of slip-velocity of the frictional strength. Further, as the frictional strength depends on the normal stress (Niemeijer et al., 2011), e.g., by affecting the frictional heating (Ashby et al., 1991), the PV-factor is suited to represent the shear loading conditions and to differentiate between different mechanisms of frictional weakening (Niemeijer et al., 2012).

The mutual dependence of frictional strength of both σ_n and V is demonstrated by a friction-map for carbonate faults (dolomites and limestones) in Fig. 6a that displays the friction-coefficient for the loading range of $0.4\ \text{MPa} < \sigma_n < 50$ MPa, and $0.001\ \text{m/s} < V < 6.5$ m/s (Table 2). One can identify three friction regimes that are separated by two lines of constant PV, $PV = 0.05\ MW/m^2$ (left boundary), where lower PV is associated with regime of high friction, and $PV = 1\ MW/m^2$ (right boundary), where higher PV is associated with regime of low friction.

While carbonate faults show monotonic relations of frictional strength with PV increase (Fig. 6a), the granitic faults display

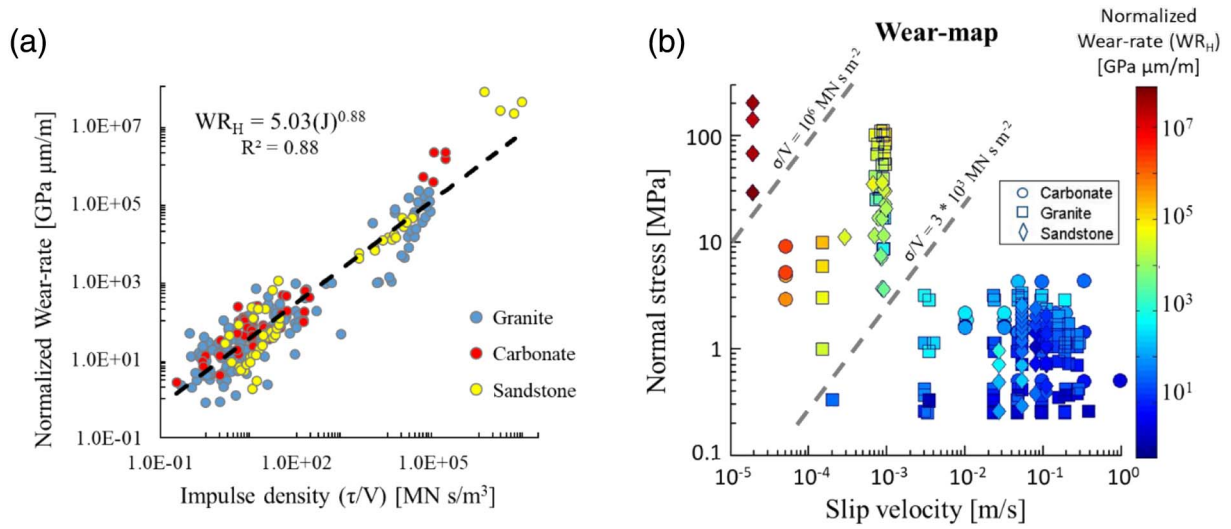

Fig. 5. (a) Normalized wear-rate, WR_H (see text) of three rock types, granites, carbonates and sandstones as function of the experimental loading represented by the ratio [shear-stress/slip-velocity]. (b) Wear-map showing the data of (a) in space of normal stress – slip velocity; note three groups of wear-rate intensity (colour scale) separated by upper and lower grey lines of constant $(\sigma/V) = 10^6$ [MN s m^{-2}] and $(\sigma/V) = 3*10^3$ [MN s m^{-2}], respectively.

nonmonotonic relations. Data from 16 studies are compiled in Fig. 6b (for experiments details see Table. 2 and Fig. A1 in the appendix) showing both the carbonate faults and granite faults friction coefficient as a function of PV-factor. Carbonate faults remain relatively strong with $\mu > 0.7$ for PV < 0.01 MW/m^2, and gradually weaken as PV exceeds 0.01 MW/m^2 as also seen in Fig. 6b. Granitic faults are relatively strong ($\mu > 0.6$) for PV below 0.005 MW/m^2, the faults weaken abruptly in the PV range of 0.005–0.05 MW/m^2, the faults strengthen gradually in PV range of 0.05–1 MW/m^2, and finally weaken for higher PV. It is evident from Fig. 6b that under similar (medium, to high) PV conditions, carbonates and granites faults display almost inverted trends of weakening-strengthening. At low PV both granite and calcite behave quasi-constant with friction around the Byerlee-law range of 0.6–0.8 (Byerlee, 1978). However, granites start to weaken before carbonates, reaching friction of 0.2–0.4, while carbonate faults have friction around 0.8. At that point, there is an opposite trend, in which carbonates weaken for PV conditions for which granite strengthen, until granite weakens again.

This remarkable difference between these rock types can be explained by the differences in the micron-scale deformation mechanics at of the gouge and slip surfaces. Carbonates weakens at high dissipated energy by plastic flow and decomposition processes that produces localization of deformation, nano-scale particles, and highly smooth 'mirror' slip surface (Boneh et al., 2013; Chen et al., 2013; Fondriest et al., 2013; Green II et al., 2015; Han et al., 2010; Siman-Tov et al., 2015; Siman-Tov et al., 2013). On the other hand, granite weakening was attributed to silica gel formation (Di Toro et al., 2004), and powder lubrication (Reches and Lockner, 2010). Subsequent strengthening and the second stage of weakening was related to the strength evolution of powder lubrication in tribology (Heshmat and Heshmat, 1999), the dehydration of water on the fine-grains of the gouge (Liao et al., 2014; Reches and Lockner, 2010; Sammis et al., 2011), or local melting (Chen et al., 2017b).

5. Relations between friction coefficient and wear-rate

In the present study, we analyzed the tribological parameters of friction coefficient and wear-rate for three groups of rocks under steady-state slip. The wear-rate data (Fig. 5) and the friction coefficient data (Fig. 6) revealed systematic relations over orders of magnitude of loading conditions. However, these data pose a puzzling relation: the wear-rate is proportional to the ratio of shear-stress to slip-velocity (τ/

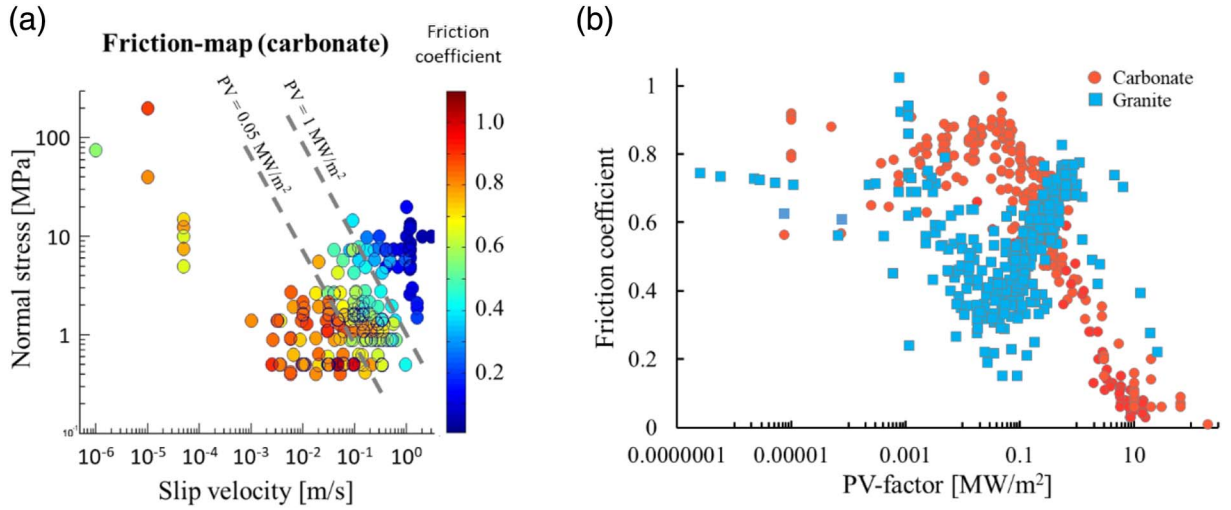

Fig. 6. (a) Friction-map for carbonates rocks displayed by friction coefficient (colour scale on the right) in space of normal stress – slip velocity. (b) Friction coefficients of shear experiments along granitic faults (blue) and carbonate faults (orange) as function of PV-factor. Experimental data is listed in Table 2 and Fig. A1 in the appendix.

Table 2
List of studies and their range of mechanical conditions used to construct the friction-coefficient graphs in Fig. 6.

	Lithology	Normal stress [Mpa]	Velocity [m/s]
Badt et al. (2016)	Hebron Limestone	5.0–15	0.00001
Boneh et al. (2013); Boneh and Reches (2016)	Dover limestone; Kasota dolomite; Blue quartzite on Kaosta dolomite; Sierra White granite	0.37–3.15	0.0002–0.37
Di Toro et al. (2004)	Westerly granite	5	0.0006–0.64
Di Toro et al. (2006)	Tonalite	5.0–20.0	1.28
Dieterich (1978)	Westerly granite	1.96	$1.3\ 10^{-7}$ - $1.5\ 10^{-4}$
Han et al. (2010)	Carrara marble; Dolomite marble (Italy); Calcite marble (Korea)	0.6–14.7	0.3–1.6
Hirose et al. (2012)	Inada granite	0.35–3.35	0.053–0.27
Liao et al. (2014)	Radiant granite	1.0–11.5	0.0006–0.27
Fukuyama and Mizoguchi (2010)	Inada granite	0.55–3.05	$7.3\ 10^{-4}$ - 0.088
Nielsen et al. (2016)	Carrara marble	30	6.5
Reches and Lockner (2010)	Sierra White granite	3.1–4.7	0.001–1.0
Siman-Tov et al. (2015)	Kfar Giladi limestone; Brown Lüder limestone; Dover Grey limestone	0.5–1.5	0.002–0.63
Tesei et al. (2017)	Mljat limestone	$1.0\ 10^{-5}$	$1.0\ 10^{-5}$
Violay et al. (2013)	Carrara marble	10	0.3–6.5
Weeks and Tullis (1985)	Dolomite marble; Granite	75	$1.0\ 10^{-7}$ - $1.0\ 10^{-6}$

V) whereas the friction-coefficient is proportional to the product of stress and velocity (σ·V). Our present model shows that wear-rate can be explained and quantified by using the single assumption that wear occurs by brittle fracturing and fragmentation of asperities of all types. On the other hand, friction is complicated as stated by Bowden and Tabor (1973) (above) "… friction is simple to measure (but) it is complicated to explain.." Macroscopic friction data integrate multiple, interacting processes that cannot be easily separated and are difficult to quantify. Yet, one exception might be related to the early stage of slip as discussed below.

We studied the evolution of friction and wear (Boneh et al., 2014) and found that during the running-in stage (early slip stage), the reduction of frictional strength strongly correlates with wear and rock comminution (Fig. 7). This relation is manifested by the almost linear proportionality between friction reduction distance (d_W) and wear-rate reduction distance (L_0). The experimental frictional work, W_f, is the sum of frictional heat, Q, and fracture surface energy associated with wear, U_s,

$$W_f = \tau u = Q + U_s \quad (17)$$

where τ and u are the shear stress and slip distance, respectively. We argued (Boneh et al., 2014) that during the slip distance interval of $u < d_W \approx L_0$ (Fig. 7b), the asperity failure and comminution dissipates a significant component of the total work, and thus becomes a major portion of the macroscopic frictional strength. Then, at steady-state with $u > d_W \approx L_0$ the wear-rate drops (Fig. 7a) with the corresponding reduction of U_s, and this effect reduces W_f and the associated friction coefficient. We note that while many studies (including the present) consider frictional strength and wear-rate at steady-state, 'true' steady-state is not necessarily reached for practical experimental limitations (Blau, 2015; Power et al., 1988). Further, as compressive strength and frictional strength are scale dependent (e.g., Weiss et al., 2014; Yamashita et al., 2015), it is possible that wear-rate is also scale dependence; to the best of our knowledge, this dependence has not been investigated.

In summary, it is expected that wear-rate and friction coefficient would be proportional to each other when energy dissipation by fracturing is relatively large, e.g., during early slip along rough fault. During steady-state, asperity fracturing is less intense (Boneh et al., 2014; Lyakhovsky et al., 2014), and the frictional work is dissipated primarily by frictional heat and plastic deformation mechanism.

6. Summary and conclusions

Analytical tools of tribology can be effectively adopted to the analysis of fault shear behavior and we propose to establish Geotribology as a sub-field in geosciences. In the present study, we demonstrate the effectiveness of geotribological approach for the derivation of a wear-rate model, and for the investigation of controlling parameters of frictional strength. The examination of wear and friction data from tens of experimental studies led to the following conclusions:

- It was widely observed that the wear of brittle faults by fracturing and fragmentation generates a gouge layer that separates the fault blocks. This process transfers a fault into a three-body system in which wear occurs at *effective asperities* that evolve with slip-

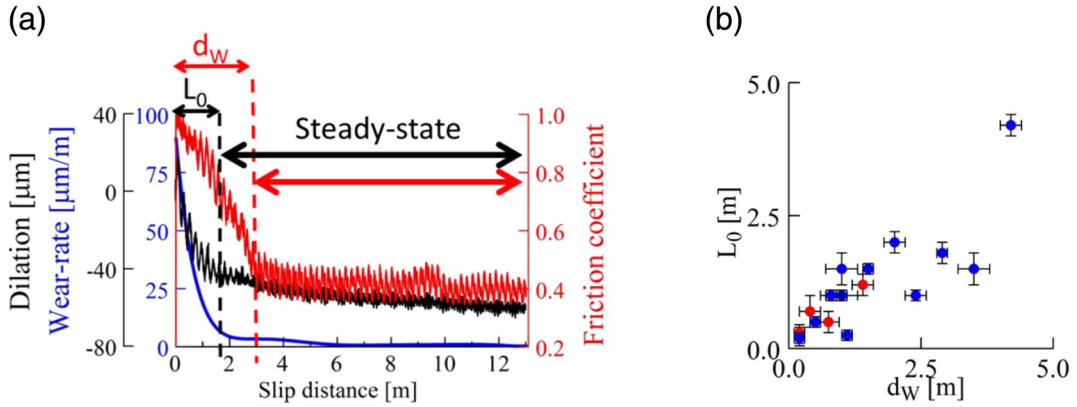

Fig. 7. (a) Evolution of friction coefficient (red), total wear (black), and wear-rate (blue) with slip distance (after experiment SWG661 in Boneh et al., 2014). Note the similarity between the transient distance of the friction, d_w, and wear, L_0, curves toward the steady-state stage. (b) The relation between transient distances of the friction coefficient (d_W), and wear (L_0); note that the two distances are linearly related to each other with a slope close to 1. After Boneh et al. (2014).

distance and develop effective roughness that may differ by scale and amplitude from the bare fault roughness.

- The present theoretical model indicates that fault wear-rate depends on the impulse-density that is the integrated force-over-time at effective asperities. The model predicts that the wear-rate, WR, is proportional to the ratio of τ/V = [shear-stress/slip-velocity], in the form, $WR = (C)(\tau/V)^b$, where C is a material constant, proportional to the inverse of the material hardness.
- We applied the model prediction to wear-rate data from granitic, carbonates and sandstone shear experiments, and found good fit over six orders of magnitudes with $b \approx 1$ for the three rock types.
- The present model incorporates slip-velocity, and thus removes major limitation of previous wear models, and further, the model provides a single, predictive function to a wide range of rocks and slip conditions. We thus envision it as a universal wear model for brittle faults.
- The compilation of dynamic friction coefficient from 23 experimental series indicates that the weakening and/or strengthening of carbonates and granitic faults are best delineated by using the tribological tools of: (a) PV-factor, which is the product normal-stress and slip-velocity; (b) Friction-maps and wear-maps that present the experimental data in loading condition space.

Acknowledgements

The present analysis was benefited from insightful discussions with Amir Sagy and Xiaofeng Chen. The authors acknowledge the thorough and constructive reviews by Takehiro Hirose and an anonymous reviewer. The work was supported, in part, by NSF Geophysics awards 1620330 and 1345087 and NEHRP award G13AP00048 to Ze'ev Reches, University of Oklahoma. The views and conclusions contained in this document are those of the authors and should not be interpreted as necessarily representing the official policies, either expressed or implied, of the U.S. Government.

Appendix A

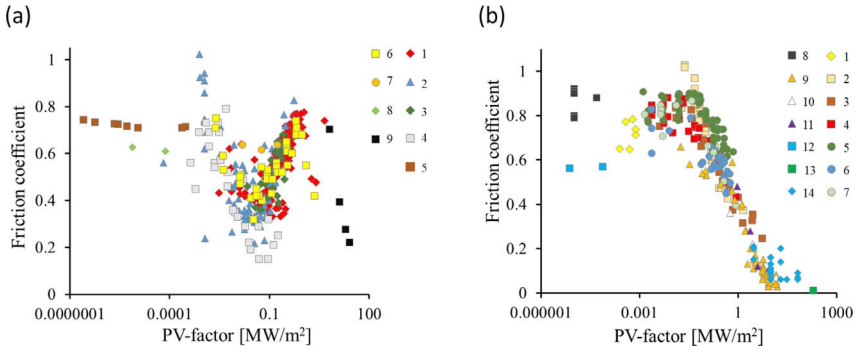

Fig. A1. Friction coefficient as a function of the experimental PV-factor (normal stress slip-velocity) for granitic (a) and carbonate (b) faults. Data sources for (a): 1 – Reches and Lockner, 2010; Sierra White granite; 2 – Boneh and Reches, 2016; Sierra White granite; 3 – Hirose et al., 2012; Inada granite; 4 – Fukuyama and Mizoguchi, 2010; Inada granite; 5 – Dieterich, 1978; Westerly granite; 6 – Liao et al., 2014; Radiant granite; 7 – Di Toro et al., 2004; Westerly granite; 8 – Weeks and Tullis, 1985; granite; 9 – Di Toro et al., 2006; Tonalite. Data sources for (b) (Table 2): 1 - Badt et al., 2016; Hebron limestone; 2 – Boneh et al., 2013; Kasota dolomite; 3 – Boneh et al., 2013; Kasota dolomite on Blue quartzite; 4 – Boneh et al., 2013; Dover limestone; 5 – Siman-Tov et al., 2015; Kfar-Giladi limestone; 6 - Siman-Tov et al., 2015; Brown Luder limestone; 7 - Siman-Tov et al., 2015; Dover Grey limestone; 8 - Tesei et al., 2017; Mljat limestone; 9 - Han et al., 2010; Carrara marble; 10 - Han et al., 2010; Dolomite marble (Italy); 11 - Han et al., 2010; Calcite marble (Korea); 12 – Weeks and Tullis, 1985; Dolomite marble; 13 – Nielsen et al., 2016; Carrara marble; 14 – Violay et al., 2013; Carrara marble. (For interpretation of the references to colour in this figure legend, the reader is referred to the web version of this article.)

References

Adachi, K., Hutchings, I., 2005. Sensitivity of wear rates in the micro-scale abrasion test to test conditions and material hardness. Wear 258, 318–321.
Adachi, K., Kato, K., Chen, N., 1997. Wear map of ceramics. Wear 203, 291–301.
Al-Qutub, A.M., Allam, I.M., Abdul Samad, M., 2008. Wear and friction of Al–Al_2O_3 composites at various sliding speeds. J. Mater. Sci. 43, 5797–5803.
Amitrano, D., Schmittbuhl, J., 2002. Fracture roughness and gouge distribution of a granite shear band. J. Geophys. Res. Solid Earth 107 (B12).
Archard, J., 1953. Contact and rubbing of flat surfaces. J. Appl. Phys. 24, 981–988.
Archard, J., Hirst, W., 1956. The wear of metals under unlubricated conditions. Proc. R. Soc. London, Ser. A 397–410 The Royal Society.
Ashby, M., Lim, S., 1990. Wear-mechanism maps. Scr. Metall. Mater. 24, 805–810.
Ashby, M., Abulawi, J., Kong, H., 1991. Temperature maps for frictional heating in dry sliding. Tribol. Trans. 34, 577–587.
Badt, N., Hatzor, Y.H., Toussaint, R., Sagy, A., 2016. Geometrical evolution of interlocked rough slip surfaces: the role of normal stress. Earth Planet. Sci. Lett. 443, 153–161.
Bai, M., Xue, Q., Guo, H., 1996. Reciprocal sliding wear of SiC particle-reinforced Al-Cu aluminium matrix composites against stainless steel, high speed tool steel and ceramics II. Wear mechanisms. Wear 194, 126–136.
Barker, L., Butcher, B., Lundergan, C., Munson, D., 1964. Influence of stress history on time-dependent spall in metals. AIAA J. 2, 977–990.
Beeman, M., Durham, W., Kirby, S., 1988. Friction of ice. J. Geophys. Res. Solid Earth 93, 7625–7633.
Bishop, R., Hill, R., Mott, N., 1945. The theory of indentation and hardness tests. Proc. Phys. Soc. 57, 147.
Blau, P.J., 2015. How common is the steady-state? The implications of wear transitions for materials selection and design. Wear 332, 1120–1128.
Blok, H., 1940. Fundamental Mechanical Aspects of Boundary Lubrication. (SAE Technical Paper).
Blok, H., 1963. The flash temperature concept. Wear 6, 483–494.
Boneh, Y., 2012. Wear and Gouge along Faults: Experimental and Mechanical Analysis. (M.S. thesis, University of Oklahoma).
Boneh, Y., Reches, Z., 2016. Wear of geo-materials by mechanical impulse. In: 50th US Rock Mechanics/Geomechanics Symposium. American Rock Mechanics Association.
Boneh, Y., Sagy, A., Reches, Z., 2013. Frictional strength and wear-rate of carbonate faults during high-velocity, steady-state sliding. Earth Planet. Sci. Lett. 381, 127–137.
Boneh, Y., Chang, J.C., Lockner, D.A., Reches, Z., 2014. Evolution of wear and friction along experimental faults. Pure Appl. Geophys. 1–17.
Bouzid, S., Nyoungue, A., Azari, Z., Bouaouadja, N., Pluvinage, G., 2001. Fracture criterion for glass under impact loading. Int. J. Impact Eng. 25, 831–845.
Bowden, F., Tabor, D., 1939. The area of contact between stationary and between moving surfaces. Proc. R. Soc. Lond. A Math. Phys. Sci. 169, 391–413.
Bowden, F.P., Tabor, D., 1964. The Friction and Lubrication of Solids. vol. 2 OUP.
Bowden, F.P., Tabor, D., 1973. Friction: An Introduction to Tribology. RE Krieger Publishing Company.
Brodsky, E.E., Gordeev, E., Kanamori, H., 2003. Landslide basal friction as measured by seismic waves. Geophys. Res. Lett. 30.
Brown, K.M., Fialko, Y., 2012. /Melt welt/'mechanism of extreme weakening of gabbro at seismic slip rates. Nature 488, 638–641.
Broz, M.E., Cook, R.F., Whitney, D.L., 2006. Microhardness, toughness, and modulus of Mohs scale minerals. Am. Mineral. 91 (1), 135–142.
Byerlee, J.D., 1967. Theory of friction based on brittle fracture. J. Appl. Phys. 38, 2928–2934.
Byerlee, J., 1978. Friction of rocks. Pure Appl. Geophys. 116, 615–626.
Candela, T., Renard, F., Bouchon, M., Schmittbuhl, J., Brodsky, E.E., 2011. Stress drop during earthquakes: effect of fault roughness scaling. Bull. Seismol. Soc. Am. 101, 2369–2387.
Chen, X., Madden, A.S., Bickmore, B.R., Reches, Z.e., 2013. Dynamic weakening by nanoscale smoothing during high-velocity fault slip. Geology 41 (7), 739–742.
Chen, X., Elwood Madden, A.S., Reches, Z.e., 2017a. The frictional strength of talc gouge

in high-velocity shear experiments. J. Geophys. Res. Solid Earth 122, 3661–3676.
Chen, X., Elwood Madden, A.S., Reches, Z.E., 2017b. Friction evolution of granitic faults: heating controlled transition from powder lubrication to frictional melt. J. Geophys. Res. Solid Earth.
Chester, F.M., Evans, J.P., Biegel, R.L., 1993. Internal structure and weakening mechanisms of the San Andreas fault. J. Geophys. Res. Solid Earth 98, 771–786.
Conway, J.C., Pangborn, R.N., Cohen, P.H., Love, D.A., 1988. Dry sliding wear behavior of an Si-Al-ON ceramic. Wear 126, 79–90.
Di Toro, G., Goldsby, D.L., Tullis, T.E., 2004. Friction falls towards zero in quartz rock as slip velocity approaches seismic rates. Nature 427, 436–439.
Di Toro, G., Hirose, T., Nielsen, S., Shimamoto, T., 2006. Relating high-velocity rock-friction experiments to coseismic slip in the presence of melts. Earthquakes: Radiated Energy and the Physics of Faulting. pp. 121–134.
Di Toro, G., Han, R., Hirose, T., De Paola, N., Nielsen, S., Mizoguchi, K., Ferri, F., Cocco, M., Shimamoto, T., 2011. Fault lubrication during earthquakes. Nature 471, 494–498.
Dieterich, J.H., 1978. Time-dependent friction and the mechanics of stick-slip. Pure Appl. Geophys. 116 (4–5), 790–806.
Dieterich, J.H., 1979. Modeling of rock friction: 1. Experimental results and constitutive equations. J. Geophys. Res. Solid Earth 84, 2161–2168.
Dieterich, J.H., Kilgore, B.D., 1994. Direct observation of frictional contacts: new insights for state-dependent properties. Pure Appl. Geophys. 143, 283–302.
Dove, J.E., Jarrett, J.B., 2002. Behavior of dilative sand interfaces in a geotribology framework. J. Geotech. Geoenviron. 128, 25–37.
Dunn, D.E., LaFountain, L.J., Jackson, R.E., 1973. Porosity dependence and mechanism of brittle fracture in sandstones. J. Geophys. Res. 78, 2403–2417.
Engelder, J.T., 1974. Cataclasis and the generation of fault gouge. Geol. Soc. Am. Bull. 85, 1515–1522.
Engelder, J., Scholz, C., 1976. The role of asperity indentation and ploughing in rock friction—II: Influence of relative hardness and normal load. Int. J. Rock Mech. Min. Sci. Geomech. Abstr. 155–163 Elsevier.
Enomoto, Y., 2005. Geotribology of earthquakes. Japanese. J. Tribol. 50, 513–521.
Enomoto, Y., Akai, M., Hashimoto, H., Mori, S., Asabe, Y., 1993. Exoelectron emission: possible relation to seismic geo-electromagnetic activities as a microscopic aspect in geotribology. Wear 168, 135–142.
Ferlito, C., Siewert, J., 2006. Lava channel formation during the 2001 eruption on Mount Etna: evidence for mechanical erosion. Phys. Rev. Lett. 96, 028501.
Fleming, J., Suh, N., 1977. Mechanics of crack propagation in delamination wear. Wear 44, 39–56.
Fondriest, M., Smith, S.A., Candela, T., Nielsen, S.B., Mair, K., Di Toro, G., 2013. Mirror-like faults and power dissipation during earthquakes. Geology 41, 1175–1178.
Fukuyama, E., Mizoguchi, K., 2010. Constitutive parameters for earthquake rupture dynamics based on high-velocity friction tests with variable sliprate. Int. J. Fract. 163 (1), 15–26.
Godet, M., 1984. The third-body approach: a mechanical view of wear. Wear 100, 437–452.
Goldsmith, W., Sackman, J., Ewerts, C., 1976. Static and dynamic fracture strength of Barre granite. Int. J. Rock Mech. Min. Sci. Geomech. Abstr. 303–309 Elsevier.
Goren, L., Aharonov, E., 2007. Long runout landslides: the role of frictional heating and hydraulic diffusivity. Geophys. Res. Lett. 34.
Green II, H., Shi, F., Bozhilov, K., Xia, G., Reches, Z., 2015. Phase transformation and nanometric flow cause extreme weakening during fault slip. Nat. Geosci. 8, 484–489.
Han, R., Hirose, T., Shimamoto, T., 2010. Strong velocity weakening and powder lubrication of simulated carbonate faults at seismic slip rates. J. Geophys. Res. Solid Earth 115.
Heshmat, H., 1991. The rheology and hydrodynamics of dry powder lubrication. Tribol. Trans. 34, 433–439.
Heshmat, H., Heshmat, C.A., 1999. On the rheodynamics of powder lubricated journal bearing: theory and experiment. Tribology Series 36, 537–549.
Hirose, T., Mizoguchi, K., Shimamoto, T., 2012. Wear processes in rocks at slow to high slip rates. J. Struct. Geol. 38, 102–116.
Hsu, S., Shen, M., 1996. Ceramic wear maps. Wear 200, 154–175.
Hsu, S.M., Shen, M., 2004. Wear prediction of ceramics. Wear 256, 867–878.
Hundley-Goff, E.M., Moody, J.B., 1980. Microscopic characteristics of orthoquartzite from sliding friction experiments. I. Sliding surface. Tectonophysics 62, 279–299.
Hutchings, I.M., 1992. Ductile-brittle transitions and wear maps for the erosion and abrasion of brittle materials. J. Phys. D. Appl. Phys. 25, A212.
Iverson, R.M., 1997. The physics of debris flows. Rev. Geophys. 35, 245–296.
Jackson, R.E., Dunn, D.E., 1974. Experimental sliding friction and cataclasis of foliated rocks. Int. J. Rock Mech. Min. Sci. Geomech. Abstr. 235–249 Elsevier.
Jost, P., 1976. Economic impact of tribology. In: Proc Mechanical Failures Prevention Group, pp. 117–139.
Kaneko, R., 2000. Some recent progress in microtribology in Japan. Tribol. Lett. 9, 89–96.
Karimi, A., Schmid, R., 1992. Ripple formation in solid-liquid erosion. Wear 156, 33–47.
Kato, K., 2002. Classification of wear mechanisms/models. Proc. Inst. Mech. Eng. B J. Eng. Tribology 216, 349–355.
LaFountain, L.J., Swain, M.V., Jackson, R.E., 1975. Origin of macroscopic wear grooves generated during sliding friction experiments. Int. J. Rock Mech. Min. Sci. Geomech. Abstr. 367–371 Elsevier.
Lawn, B.R., 1975. A model for the wear of brittle solids under fixed abrasive conditions. Wear 33, 369–372.
Lee, A., Rutter, E., 2004. Experimental rock-on-rock frictional wear: application to subglacial abrasion. J. Geophys. Res. Solid Earth 109.
Liao, Z., Chang, J.C., Reches, Z.e., 2014. Fault strength evolution during high velocity friction experiments with slip-pulse and constant-velocity loading. Earth Planet. Sci. Lett. 406, 93–101.
Lim, S., Ashby, M., 1987. Overview no. 55 wear-mechanism maps. Acta Metall. 35, 1–24.
Lindholm, U., Yeakley, L., Nagy, A., 1974. The dynamic strength and fracture properties of dresser basalt. Int. J. Rock Mech. Min. Sci. Geomech. Abstr. 181–191 Elsevier.
Lyakhovsky, V., Sagy, A., Boneh, Y., Reches, Z.e., 2014. Fault wear by damage evolution during steady-state slip. Pure Appl. Geophys. 1–15.
Marone, C., 1998. Laboratory-derived friction laws and their application to seismic faulting. Annu. Rev. Earth Planet. Sci. 26, 643–696.
Moore, M., King, F., 1980. Abrasive wear of brittle solids. Wear 60, 123–140.
Nielsen, S., Spagnuolo, E., Smith, S.A.F., Violay, M., Di Toro, G., Bistacchi, A., 2016. Scaling in natural and laboratory earthquakes. Geophys. Res. Lett. 43 (4), 1504–1510.
Niemeijer, A., Di Toro, G., Nielsen, S., Di Felice, F., 2011. Frictional melting of gabbro under extreme experimental conditions of normal stress, acceleration, and sliding velocity. J. Geophys. Res. Solid Earth 116.
Niemeijer, A., Di Toro, G., Griffith, W.A., Bistacchi, A., Smith, S.A., Nielsen, S., 2012. Inferring earthquake physics and chemistry using an integrated field and laboratory approach. J. Struct. Geol. 39, 2–36.
Power, W.L., Tullis, T.E., Weeks, J.D., 1988. Roughness and wear during brittle faulting. J. Geophys. Res. Solid Earth 93, 15268–15278.
Qian, Q., Qi, C., Wang, M., 2009. Dynamic strength of rocks and physical nature of rock strength. J. Rock Mech. Geotech. Eng. 1, 1–10.
Queener, C., Smith, T., Mitchell, W., 1965. Transient wear of machine parts. Wear 8, 391–400.
Rabinowicz, E., 1965. Friction and Wear of Materials.
Rabinowicz, E., Dunn, L., Russell, P., 1961. A study of abrasive wear under three-body conditions. Wear 4, 345–355.
Ramalho, A., Miranda, J., 2006. The relationship between wear and dissipated energy in sliding systems. Wear 260, 361–367.
Reches, Z.e., Lockner, D.A., 2010. Fault weakening and earthquake instability by powder lubrication. Nature 467, 452–455.
Renard, F., Mair, K., Gundersen, O., 2012. Surface roughness evolution on experimentally simulated faults. J. Struct. Geol. 45, 101–112.
Rice, J.R., 2006. Heating and weakening of faults during earthquake slip. J. Geophys. Res. Solid Earth 111.
Rozeanu, L., 1963. Fatigue wear as a rate process. Wear 6, 337–340.
Sagy, A., Brodsky, E.E., 2009. Geometric and rheological asperities in an exposed fault zone. J. Geophys. Res. Solid Earth 114.
Sagy, A., Brodsky, E.E., Axen, G.J., 2007. Evolution of fault-surface roughness with slip. Geology 35, 283–286.
Sagy, A., Tesei, T., Collettini, C., 2017. Fault-surface geometry controlled by faulting mechanisms: experimental observations in limestone faults. Geology 45, 851–854.
Sammis, C.G., Lockner, D.A., Reches, Z.e., 2011. The role of adsorbed water on the friction of a layer of submicron particles. Pure Appl. Geophys. 168, 2325–2334.
Scholz, C.H., 1987. Wear and gouge formation in brittle faulting. Geology 15, 493–495.
Shervais, K.A., Kirkpatrick, J.D., 2016. Smoothing and re-roughening processes: the geometric evolution of a single fault zone. J. Struct. Geol. 91, 130–143.
Shockey, D., Erlich, D., Kalthoff, J., Homma, H., 1986. Short-pulse fracture mechanics. Eng. Fract. Mech. 23, 311–319.
Siman-Tov, S., Aharonov, E., Sagy, A., Emmanuel, S., 2013. Nanograins form carbonate fault mirrors. Geology 41, 703–706.
Siman-Tov, S., Aharonov, E., Boneh, Y., Reches, Z.e., 2015. Fault mirrors along carbonate faults: formation and destruction during shear experiments. Earth Planet. Sci. Lett. 430, 367–376.
Srinivasan, S., Scattergood, R.O., 1988. Effect of erodent hardness on erosion of brittle materials. Wear 128, 139–152.
Subramanian, C., 1991. Effects of sliding speed on the unlubricated wear behaviour of Al-12.3 wt.% Si alloy. Wear 151, 97–110.
Suh, N.P., 1973. The delamination theory of wear. Wear 25, 111–124.
Tesei, T., Carpenter, B.M., Giorgetti, C., Scuderi, M.M., Sagy, A., Scarlato, P., Collettini, C., 2017. Friction and scale-dependent deformation processes of large experimental carbonate faults. J. Struct. Geol. 12–23.
Teufel, L., 1981. Pore volume changes during frictional sliding of simulated faults. In: Mechanical Behavior of Crustal Rocks: The Handin Volume, pp. 135–145.
Tsutsumi, A., Shimamoto, T., 1997. High-velocity frictional properties of gabbro. Geophys. Res. Lett. 24, 699–702.
Tuler, F.R., Butcher, B.M., 1968. A criterion for the time dependence of dynamic fracture. Int. J. Fract. Mech. 4, 431–437.
Violay, M., Nielsen, S., Spagnuolo, E., Cinti, D., Di Toro, G., Di Stefano, G., 2013. Pore fluid in experimental calcite-bearing faults: abrupt weakening and geochemical signature of co-seismic processes. Earth Planet. Sci. Lett. 361, 74–84.
Wang, W., Scholz, C.H., 1994. Wear processes during frictional sliding of rock: a theoretical and experimental study. J. Geophys. Res. 99, 6789–6799 -ALL SERIES-.
Watson, S., Friedersdorf, F., Madsen, B., Cramer, S., 1995. Methods of measuring wear-corrosion synergism. Wear 181, 476–484.
Weeks, J.D., Tullis, T.E., 1985. Frictional sliding of dolomite: a variation in constitutive behavior. J. Geophys. Res. Solid Earth 90 (B9), 7821–7826.
Weiss, J., Girard, L., Gimbert, F., Amitrano, D., Vandembroucq, D., 2014. (Finite) statistical size effects on compressive strength. Proc. Natl. Acad. Sci. 111, 6231–6236.
Williams, J.A., 2005. Wear and wear particles—some fundamentals. Tribol. Int. 38, 863–870.
Yamamoto, T., Olsson, M., Hogmark, S., 1994. Three-body abrasive wear of ceramic materials. Wear 174, 21–31.
Yamashita, F., Fukuyama, E., Mizoguchi, K., 2014. Probing the slip-weakening mechanism of earthquakes with electrical conductivity: rapid transition from asperity contact to gouge comminution. Geophys. Res. Lett. 41, 341–347.
Yamashita, F., Fukuyama, E., Mizoguchi, K., Takizawa, S., Xu, S., Kawakata, H., 2015.

Scale dependence of rock friction at high work rate. Nature 528, 254–257.
Yoshioka, N., 1986. Fracture energy and the variation of gouge and surface roughness during frictional sliding of rocks. J. Phys. Earth 34, 335–355.
Zhang, J., Alpas, A., 1997. Transition between mild and severe wear in aluminium alloys. Acta Mater. 45, 513–528.
Zhang, Q., Zhao, J., 2013. Effect of loading rate on fracture toughness and failure micromechanisms in marble. Eng. Fract. Mech. 102, 288–309.
Zhang, Q., Zhao, J., 2014. A review of dynamic experimental techniques and mechanical behaviour of rock materials. Rock Mech. Rock. Eng. 47, 1411.
Zhang, Z., Kou, S., Yu, J., Yu, Y., Jiang, L., Lindqvist, P.-A., 1999. Effects of loading rate on rock fracture. Int. J. Rock Mech. Min. Sci. 36, 597–611.
Zum Gahr, K., 1988. Modelling of two-body abrasive wear. Wear 124, 87–103.